Drift resonant generation of peaked relativistic electron distributions by Pc 5 ULF waves

A. W. Degeling,[1] L. G. Ozeke,[1] R. Rankin,[1] I. R. Mann,[1] and K. Kabin[1]

Received 20 March 2007; revised 18 September 2007; accepted 15 November 2007; published 22 February 2008.

[1] The adiabatic drift-resonant interaction between relativistic, equatorially mirroring electrons and narrowband, Pc 5 ultra low frequency (ULF) waves in the magnetosphere is investigated using a time-dependent magnetohydrodynamic (MHD) wave model. Attention is focused on the effect of a ULF wave packet with finite duration on the equatorially mirroring, relativistic electron phase space density (PSD) profile. It is demonstrated that a burst of narrow band ULF waves can give rise to the growth of strong localized peaks in PSD with *L*-shell by nondiffusive radial transport. This contrasts with the diffusive "external source acceleration mechanism" described by Green and Kivelson (2004), a radial transport mechanism often attributed to ULF waves, which cannot produce peaks in PSD that increase with time. On the basis of this paradigm, observations of locally growing PSD peaks are usually attributed to very low frequency (VLF) wave acceleration by resonant interactions with lower-band chorus (e.g., Horne et al., 2005). However, we show that in situations where large amplitude, narrow bandwidth ULF waves are also observed, these time-limited coherent ULF waves can also generate growing PSD peaks and under such circumstances may offer an alternative explanation.

Citation: Degeling, A. W., L. G. Ozeke, R. Rankin, I. R. Mann, and K. Kabin (2008), Drift resonant generation of peaked relativistic electron distributions by Pc 5 ULF waves, *J. Geophys. Res.*, *113*, A02208, doi:10.1029/2007JA012411.

1. Introduction

[2] In situ measurements of outer radiation belt relativistic electron populations have on occasions during geomagnetic storms shown the formation of peaks in phase space density with *L*-shell (in particular, with the *L*-shell parameter *L** defined by *Roederer* [1970]). This has been interpreted as evidence supporting the hypothesis that the dominant source of these electrons is through local, or internal acceleration by very low frequency (VLF) waves [*Green and Kivelson*, 2004; *Horne et al.*, 2005]. In this mechanism, resonant wave-particle interactions breaking the first adiabatic invariant, for example with lower-band chorus outside the plasmapause, energize the local electron population. The longstanding, alternative hypothesis is that electrons are transported across *L*-shell by guiding-center drifts due to electric and magnetic field perturbations in the ultra low frequency (ULF) range [e.g., *Falthammer*, 1965]. The electrons gain energy through the work done in moving into a region of higher magnetic fields, preserving the first two adiabatic invariants and breaking the third. A statistical correlation between ULF wave activity and electron flux enhancements in the outer radiation belt has been established in separate studies using ground-based ULF wave power by *Rostoker et al.* [1998] and *Mathie and Mann* [2000].

[3] The energization processes in response to either broadband VLF or ULF wave power are generally considered to be diffusive by many authors dealing with this topic [*O'Brien et al.*, 2003; *Ukhorskiy et al.*, 2005; *Falthammer*, 1965; *Schulz and Lanzerotti*, 1974; *Elkington et al.*, 2003; *Brizard and Chan*, 2001; *Friedel et al.*, 2002] and modelled accordingly. The general conditions for the applicability of a diffusion model to broadband fluctuations are given by Sagdeev and Galeev [1969, section 2.2]. Briefly, the basis of a diffusive description is the following argument. Consider a population of drifting electrons (with identical first and second adiabatic invariants) interacting with a broadband ULF wave source, which may be described by the sum of a number of Fourier components with varying amplitudes. Associated with each wave component is the drift-resonance location in *L*-shell (*Elkington et al.* [1999], where the electron drift speed matches the wave phase speed, causing violation of the third adiabatic invariant) and trapping width (ΔL, associated with the wave amplitude, which separates resonant from nonresonant electrons). The overlap of trapping widths from neighboring spectral components gives rise to Brownian motion in the electron trajectories. This stochastic behavior of the electron population can be described statistically as a quasi-linear diffusive process, under the condition that the spread in resonance locations associated with the Fourier components of the broadband signal is much greater than the trapping width associated with the (integrated) signal amplitude. Similar arguments can be made in conjunction with gyroresonances and bounce resonances and broadband waves with higher frequencies.

[1]Department of Physics, University of Alberta, Edmonton, Alberta, Canada.

0148-0227/08/2007JA012411

[4] Under these conditions, [*Schulz and Lanzerotti*, 1974] argue that an "essentially complete physical description of the Earth's radiation environment" is provided by averaging the gyrophase, bounce phase, and drift phase of the electrons in order to express PSD in terms of the adiabatic invariants and time: $f = f(M, J, L, t)$ (where M and J are the first and second adiabatic invariants associated with gyromotion and bounce motion, and L represents the third invariant and is generalized to the Roederer coordinate L^* in a nonaxisymmetric geomagnetic field). The average effect of violations in the invariants can then be represented by the diffusion of f with respect to M, J, and/or L. *Green and Kivelson* [2004] apply this argument to interpret electron flux measurements from the Polar satellite and note that the observed locally growing peaks in f with L (keeping M and J constant) cannot be the result of diffusive transport across L-shell. This is because the net effect of diffusive transport is always to move electrons from regions of high phase space density to lower phase space density, which precludes the formation of growing localized peaks.

[5] There is a growing awareness of the shortcomings of diffusive models in describing radiation belt electron dynamics. *Riley and Wolf* [1992] compare convective and diffusive descriptions of electron dynamics with moderate energies (up to 130 keV at $L = 3$) using a simple electrostatic model for ULF fluctuations during a geomagnetic storm and find that the diffusion model only agrees in an ensemble average sense with the convective model (that is, the average of many runs with identical power spectra for the ULF fields but randomized initialized phases). *Ukhorskiy et al.* [2006a] investigate the effect of fluctuations in solar wind ram pressure on radiation belt dynamics and show that even though the electron motion is stochastic, it cannot be described by a diffusion equation. Similarly, *Degeling et al.* [2006] demonstrate that the localization of narrowband ULF waves in local time can lead to stochastic motion that enhances radial transport; however, the associated phase decorrelation timescale is longer than the typical duration of ULF waves, which precludes a diffusive description. *Ukhorskiy et al.* [2006b] demonstrate a convective electron transport mechanism caused by variations in the ring current and D_{st} during geomagnetic storms, which causes the adiabatic capture and subsequent release of radiation belt electrons, leading to the formation of a localized peak in phase space density.

[6] The purpose of this article is to examine adiabatic transport due to coherent, narrowband ULF compressional waves, for which the condition of validity of a diffusive description breaks down. We demonstrate that growing localized peaks in phase space density can be produced by the drift-resonant interaction between temporally limited ULF wavetrains and MeV energy electrons. These PSD peaks remain in place once the ULF wave activity has decayed away, leaving features in the PSD profile with L-shell that may easily be misdiagnosed as evidence of local electron acceleration.

[7] The waves of interest in this study are narrow-band ULF compressional waves with low azimuthal mode number m, which couple to discrete frequency field line resonances (FLRs), and are routinely observed by ground-based instruments (e.g., magnetometers and superDARN radar [*Rae et al.*, 2005; *Fenrich et al.*, 1995]). FLRs are detections of resonantly excited shear wave eigenmodes along a specific set of field lines. In the case of low-m modes, the observed eigenfrequency matches that of a compressional (fast wave) driver propagating across field lines through the magnetosphere. These compressional waves may be excited either along the dayside or flanks of the magnetopause (for example, by solar wind buffeting or Kelvin-Helmholtz instability where the solar wind flow adjacent the magnetopause is strongly sheared) and propagate within the magnetosphere until they are reflected at the compressional wave turning point [*Allan and Poulter*, 1992]. The FLR location is typically earthward of the turning point, and power is coupled to it via evanescent fields from the reflecting waves. The latitudinal width of the FLR amplitude peak places an upper bound on the bandwidth of the compressional waves to which they are coupled, if the Alfvén continuum is also known. In this case the Alfven continuum provides a mapping from the FLR width in latitude to frequency bandwidth. It represents an upper bound in bandwidth because the FLR profile in latitude is also broadened by finite ionospheric conductance.

[8] It is considered that on the dayside of the magnetosphere, compressional waves form a radial eigenmode, or waveguide, structure between the magnetopause and turning point. This may explain the apparent preference of particular observed FLR frequencies reported by *Fenrich et al.* [1995]. The extensive radial structure of compressional waves from the magnetopause to the FLR location enables the waves to interact with electrons via the drift resonance across a wide range of L-shells.

[9] In this article, a compressional wave coupled to a FLR excited from a time-dependent source at the magnetopause is modeled in a dipole magnetic field geometry and is used to perturb an initial distribution of equatorially mirroring electrons with a monotonic radial density gradient. This extends previous work of *Degeling et al.* [2006] in which monochromatic ULF eigenmodes in a box model with a time-independent amplitude were used to perturb MeV electron dynamics. The drift-resonant interaction between the wave and electrons with azimuthal drift speeds close to the wave phase speed results in nondiffusive radial transport, and the generation of a localized peak in phase space density, which is retained after the wave has decayed away. Section 2 provides an overview of the ULF wave model and further details appear in Appendix A. Section 3 describes the model for equatorially mirroring electron dynamics. The results are presented in section 4, and section 5 discusses the implications of these results on efforts to determine the mechanism of electron acceleration from in situ measurements of phase space density. The conclusions are given in section 6.

2. ULF Wave Model

[10] In this section, we overview an ideal MHD model for ULF waves in an inhomogeneous plasma representing the magnetosphere. Details of the method by which the model equations are solved are given in Appendix A. We take this particular approach in order to base the electron dynamics results that follow on electromagnetic fields derived from a physics based model that takes into account the state of the magnetospheric plasma. By treating the

ULF waves in an internally consistent manner, we avoid unphysical or unrealistic wave-particle interactions that can give erroneous electron transport and energization, particularly in the case of narrowband waves where the transport is nondiffusive. In this sense the use of our ULF wave model represents an improvement over previous approaches, which specify the wave fields a priori [e.g., *Elkington et al.*, 1999]. Additionally, the coupling of FLRs and compressional waves included in this model enables the use of ground-based observations of the amplitude, duration, and latitudinal width of FLRs to constrain the ULF wave amplitude and duration of compressional waves across a large range of L-shells, by scaling the compressional wave source parameters and ionospheric conductivity appropriately. For example, in all model runs performed in this paper, the peak radial electric field occurring at the FLR location is set no higher than 5 mV/m. This corresponds roughly with the peak Pc-5 ULF wave amplitude inferred by ground-based observations during the extreme conditions of the 2003 Halloween geomagnetic storm (peak Dst = -400 nT, solar wind speeds exceeding 1500 km/s [*Loto'aniu et al.*, 2006]).

[11] For this wave model, we use a dipole orthogonal coordinate system, defined in terms of spherical polar coordinates (r, θ, ϕ by

$$\alpha = \frac{\sin^2\theta}{r} \equiv 1/LR_E, \quad \beta = \phi, \quad \mu = \frac{\cos\theta}{r^2} \tag{1}$$

and

$$h_\alpha = \frac{r^2}{\sin\theta(1+3\cos^2\theta)^{1/2}}, h_\beta = r\sin\theta, \quad h_\mu = h_\alpha h_\beta \tag{2}$$

[12] Starting from the cold plasma MHD equations, the following wave equation for the field line displacement $\boldsymbol{\xi}$ can be obtained [*Allan and Poulter*, 1992]:

$$\left(\frac{\partial^2}{\partial t^2} + v_A^2 \nabla_\perp \times \nabla \times\right)(\boldsymbol{\xi} \times \mathbf{B_o}) = 0 \tag{3}$$

where $\mathbf{B_o}$ is the unperturbed magnetic field and $v_A^2 = B_o^2/\mu_o\rho$ is the square of the Alfvén speed (and ρ is the plasma mass density). Note that $|B_o| = B_{eq}{R_E}^3/h_\mu$, where B_{eq} is the equatorial magnetic field strength at the surface of the Earth.

[13] The method by which this equation is solved is described in Appendix A. Briefly, the equations resulting from the components of equation (3) are simplified by making the slowly varying approximation, where changes in the wave amplitude take place on a timescale that is longer than the wave period. By assuming that the Alfvén speed is a separable function in α and μ, and assuming finite Pederson conductivity for the ionospheric boundary conditions, the wave fields are described in terms of the geomagnetic field-aligned fundamental eigenfunctions for the toroidal and poloidal polarizations, leading to a set of coupled first order equations in time that are relatively easy to solve numerically. Wave-like disturbances of the form $\exp(i(m\phi - \omega t))$ (where m is the azimuthal mode number and ω is the wave frequency) occur in response to an imposed time-dependent perturbation in ξ placed at the outer L-shell boundary, for which the amplitude envelope is parameterized by $e^{-t/\tau 2}(1 - e^{-t/\tau 1})$. The constants τ_1 and τ_2 represent the ULF wave source rise and decay times, respectively. Typically, τ_1 is set to one wave period, and τ_2 is set between three and nine wave periods. For a typical wave frequency of 3.0 mHz, this range corresponds to ULF wavetrains with durations between 1 and 3 hours, which covers the range of commonly observed ULF signatures observed by ground-based instruments.

[14] Once the time-dependent field line displacements have been obtained, the electric field is given by Ohm's law: $\mathbf{E} = -\mathbf{u} \times \mathbf{B}_o$, where $\mathbf{u} = \partial\xi/\partial t$. The magnetic field is given by $\mathbf{B(t)} = \mathbf{B_o} + \mathbf{b(t)}$, where the perturbed magnetic field from Faraday's law is given by: $\mathbf{b} = \nabla \times (\xi \times \mathbf{B_o})$. The assumption of fundamental eigenfunctions along field lines implies that $\boldsymbol{\xi}$ has an antinode on the equatorial plane, and therefore $b_\parallel$ and $E_\perp$ also have equatorial antinodes, while $b_\perp$ has a node on the equatorial plane. The equatorial value of $b_\parallel$ is given by: $b_\parallel = -\nabla \cdot (\boldsymbol{\xi} B_o)$.

[15] An example of the MHD wave model output for a typical scenario is shown in Figure 1 ($m = 3$, $\omega/2\pi = 3.0$ mHz, $\rho = 800$ amu/cm^{-3} at $L = 4$, with an L^{-4} scaling). Figures 1a and 1b show the variation with time and L-shell of the amplitude of $B_o\boldsymbol{\xi}$, which is used to calculate the wave electric and magnetic fields as described above. Radial profiles of the amplitude and phase of the components of $\mathbf{E}$ and $b_\parallel$, taken at a time five periods after the source commencement, are shown in Figure 1c, and the temporal profile of the source amplitude is shown in the inset. In this figure, the disturbance at the outer boundary (L = 12) launches a compressional wave that forms a broad standing wave across L-shell and couples power to a field line resonance. The compressional wave structure grows and decays with the source, which has a rise-time τ_1 of 1 period and decays with an e-folding time τ_2 of 5 wave periods. The FLR is most visible in the top figure as a highly localized structure centered at L = 4, which corresponds to the location where the driver frequency matches the toroidal mode eigenfrequency. It grows and decays according to the balance of power input from the compressional wave and power lost by ohmic dissipation in the ionosphere (determined by the Pedersen ionospheric conductance Σ_p). This causes the FLR amplitude to peak approximately 4 wave periods after the compressional wave peak and decay with a much longer timescale than τ_2. Hence while the presence of the compressional wave may be inferred by the measurement on the ground of an FLR (with low m), the time evolution of the Alfvénic FLR amplitude does not correspond closely with that of compressional wave. This should be kept in mind when inferring ULF wave amplitudes in the magnetosphere from ground based measurements.

[16] In this paper, we are primarily interested in the effect on election phase space density of nondiffusive radial transport arising from the drift resonance interaction with the azimuthal component of the ULF electric field. We therefore restrict our attention to the effect of the compressional mode on electron dynamics at locations well away from the field line resonance, where the strongly peaked radial electric field introduces complexity to the electron dynamics that is beyond the scope of the current investigation. For example, in section 4 we examine the dynamics of drift-resonant electrons in the vicinity of geostationary orbit using the ULF wave model param-

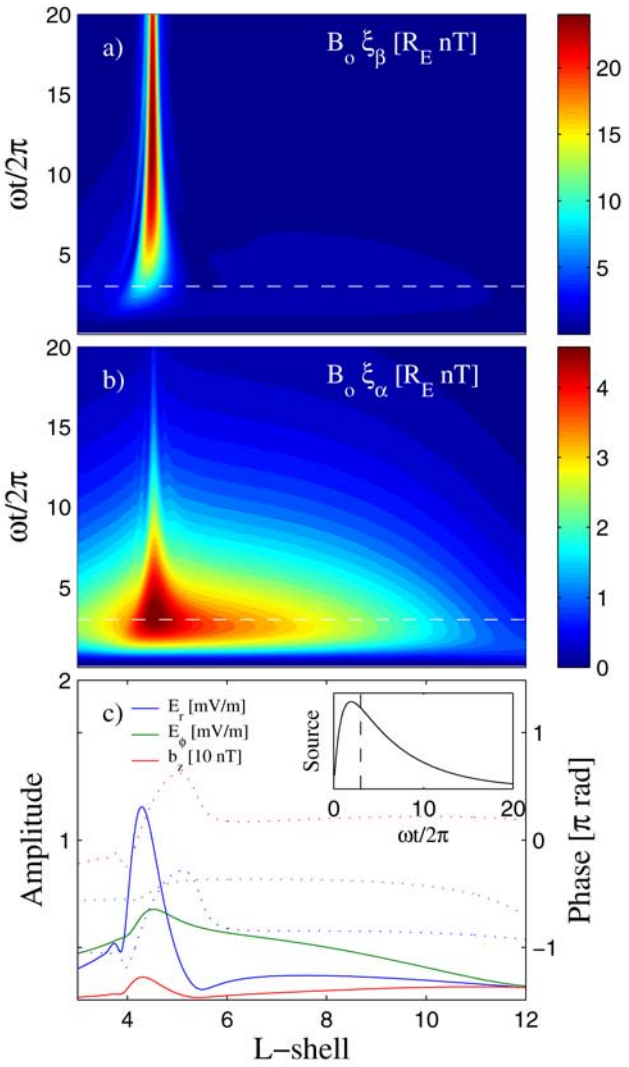

Figure 1. (a) and (b) Time evolution with L-shell of the field line displacement (ξ) in the azimuthal (β) and radial (α) directions, respectively, multiplied by B_o. The electric and magnetic fields are obtained from these data by finite differencing. (c) Also shown is the amplitude (solid) and phase (dotted) of the equatorial E_r, E_ϕ, and b_z after 5 wave periods from the commencement of the source, the temporal variation of which is shown in the inset.

eters chosen to give Figure 1, for which the usage of this simplified wave model is justified. That is, this time-dependent wave model represents the simplest internally consistent model for MHD waves in a dipole magnetic field available, which contains enough physics to give rise to physically realistic electron dynamics for the chosen scenario of interest.

3. Equatorially Mirroring Electron Dynamics

[17] The electron dynamics model used in the current study has been described previously [*Degeling et al.*, 2006], so only a brief overview is given here. In a dipole magnetic field, the equatorial plane corresponds to the surface where the mirror force parallel to the magnetic field passes through zero. Consequently, electrons with zero parallel momentum residing on the equatorial plane are confined to this plane for all time (in the absence of any other external force parallel to B) and are said to be equatorially mirroring. This reduction in the number of degrees of freedom greatly simplifies modelling their dynamics. The guiding-center drift equation derived by *Northrop* [1963] is simplified for these electrons and is given in component form (using polar coordinates (r, ϕ) in the equatorial plane) by

$$\dot{r} = \frac{E_\phi}{B} - \frac{M}{qr\gamma B}\frac{\partial B}{\partial \phi} \tag{4}$$

$$\dot{\phi} = -\frac{E_r}{rB} + \frac{M}{qr\gamma B}\frac{\partial B}{\partial r}. \tag{5}$$

In these equations, E_r and E_ϕ are the radial and azimuthal components of the electric field, B is the magnetic field strength (scalar), γ is the relativistic correction factor, and the magnetic moment (first adiabatic invariant) is given by $M = p_\perp^2/2m_eB$, where $p_\perp$ is the component of electron momentum perpendicular to the magnetic field. The first and second terms in each of the above equations correspond to the $\mathbf{E} \times \mathbf{B}$ and ∇B drifts, respectively. For reference, the total relativistic energy of an electron is given by $E_{tot} = W + m_ec^2 = \gamma m_ec^2 = (p^2c^2 + m_e^2c^4)^{1/2}$, where W is the kinetic energy. Rearranging the above equation gives $W = m_ec^2(\gamma - 1)$. Hence the kinetic energy is a function of magnetic field strength, given by $W = m_ec^2\,((1 + 2MB/m_ec^2)^{1/2} - 1)$.

[18] Equations (4) and (5) are numerically integrated using a fourth-order Runge Kutta scheme for electrons with initial locations arranged on an (r, ϕ) grid (typically with 200 grid points in each direction), with identical magnetic moment M. Trajectories are calculated over a typical time-span of 30 ULF wave periods, using the electromagnetic fields on the equatorial plane provided by the ULF wave model described in section 2. According to Liouville's theorem, the phase space density of electrons $f(M, J, L, \phi, t)$ remains constant along each trajectory in the absence of collisions. This is used to compute the evolution of f in space and time given an initial condition $f_i = f(M, J, L, \phi, t_i)$, by adopting an interpolation algorithm used as part of Vlasov Hybrid Simulations [*Nunn*, 1993]. In this procedure, evaluations of PSD (f_m) are made each time step by the interpolation of f from the trajectories onto the polar coordinate grid using a phase space area conservative algorithm. Note that any interpolation errors in f_m do not propagate because f (not f_m advected from the previous time step) is used in the interpolation. The initial condition for PSD is given by

$$f_i = \left(\frac{f_o}{L^6}\right)\exp(-W/kT_e) \tag{6}$$

where f_o is a constant, the electron temperature kT_e is set to 0.1 MeV. This gives a monotonically increasing initial PSD profile with L-shell for $L < 9$.

4. PSD Peak Generation Through Coherent Radial Transport

[19] The ULF waves shown in Figure 1 were used as inputs in the electron dynamics model described above.

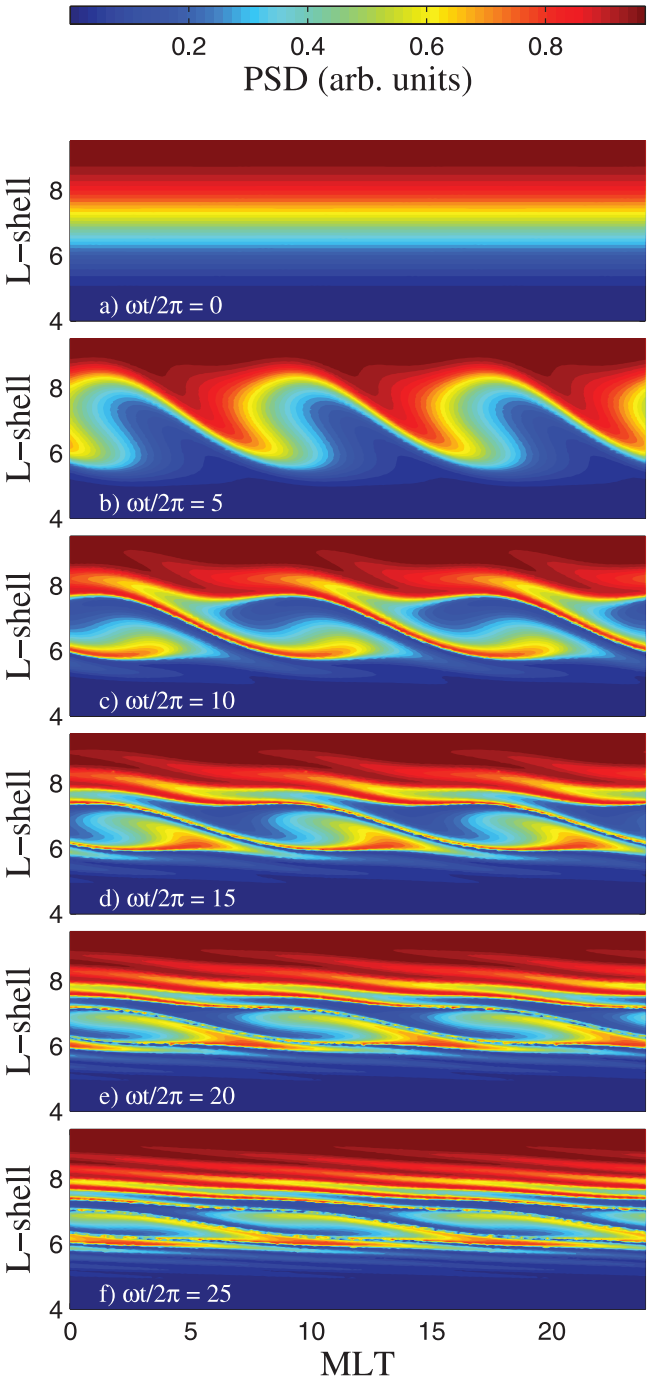

Figure 2. (a–f) Contour plots of phase space density as functions of *L*-shell and MLT for the ULF wave shown in Figure 1, taken at intervals of 5 periods.

Electrons with a constant magnetic moment of $M = 7.5$ *MeV*/μT were considered, which corresponds to a drift resonance location of $L_o = 6.6$ for the particular ULF wave parameters used. Figure 2 shows a series of phase space density (PSD) *L-MLT* profiles in the equatorial plane, at intervals of 5 wave periods following the source commencement. These images show the adiabatic transport of electrons starting from the initial condition shown in the first frame. The ULF wave considered in this case has an azimuthal mode number $m = 3$, giving rise to three identical spatial structures across 24 h of magnetic local time (MLT). These structures, forming the three red finger-like extensions in Figure 2b, propagate azimuthally and are the result of electrons becoming trapped between consecutive wavefronts. As described by *Degeling et al.* [2006], the electrons forming these structures librate around drift-resonance equilibrium points (in the anti-clockwise direction in the figure) as these points travel at the phase velocity of the wave (from left to right in the figure). As the electrons move adiabatically into the stronger magnetic field at lower *L*-shells, they gain kinetic energy in their gyromotion, which in turn causes their azimuthal drift speed to increase. Once the electrons have been transported below L_o, their drift speed exceeds the phase speed of the wave. Eventually, these electrons pass the point in phase in the wave reference frame where the wave field causing their inward radial transport changes sign. Figure 2c shows that by 10 wave periods in the example shown, the leading edge of the structures that were being transported earthward have started to move away from the Earth. These electrons are now losing some of the energy they initially gained as they move back into the weaker geomagnetic field. This also shows that the maximum extent of radial transport by the drift resonance mechanism due to a single ULF wave is limited to a specific range in *L*-shell bracketing the drift resonance location, known as the trapping width ΔL_{tr}. It can be shown [*Degeling et al.*, 2006; *Elkington et al.*, 2003] that ΔL_{tr} is proportional to the square root of the wave amplitude. If the wave amplitude were constant in time, the motion of all electrons would be completely cyclic (albeit with differing periods, known as the trapping period τ_{tr}), and there would be no net energy gain or loss for each electron over a cycle. However, as shown in Figure 1, the compressional wave amplitude used in this example reaches a peak during the first five wave periods,

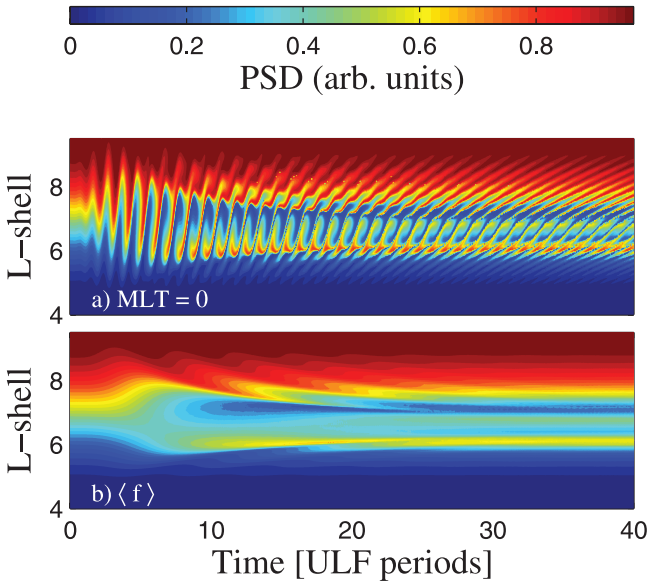

Figure 3. (a) A contour plot showing the evolution in time of the PSD as a function of *L*-shell, holding MLT = 0; (b) contour plots of the average over ϕ of PSD versus time and *L*-shell.

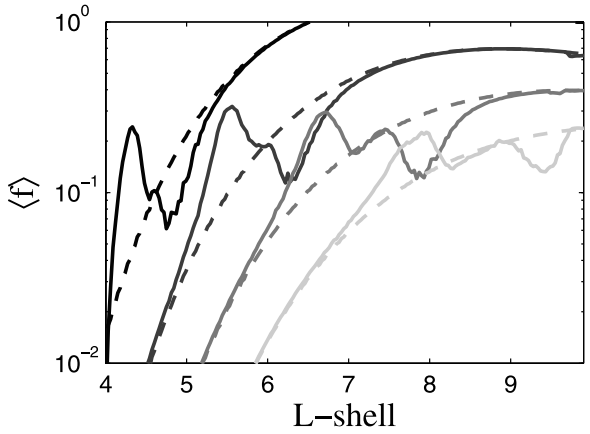

Figure 4. Radial profiles of the final phase space density taken after 30 wave periods, for the same ULF wave parameters used in the previous figures and averaged over MLT. Each curve corresponds to a different magnetic moment, for which the drift resonance locations are L = 4.6, 5.9, 7.3 and 8.6 (from dark to light grey levels). The initial profiles are shown by dashed lines.

and subsequently decays. This has the effect of reducing, and finally preventing, any further radial transport as time progresses. In this way, regions of high phase space density that are initially transported radially earthward while the ULF wave amplitude is large are left in place as the wave decays. The subsequent frames in the figure show that differences in azimuthal drift velocity with L-shell cause the azimuthal structures to become increasingly sheared with time (this may be thought of as temporal phase mixing).

[20] Figure 3a shows the time evolution of the PSD profile for a constant MLT, which corresponds to sampling data along a vertical slice (at MLT = 0) in each panel of Figure 2. This figure shows that the perturbation to PSD develops from an initial oscillation in L-shell to a spiral pattern as trapped electrons execute an increasing fraction of an orbit in the wave frame. This occurs over the first 5 to 10 wave periods while the ULF wave amplitude remains significant. Further radial transport is prevented as time continues and the wave amplitude decays, and the existing PSD structure in L-shell appears to become sheared in the time domain, due to the difference in azimuthal drift velocity with L-shell. This figure, and also the final two panels of Figure 2, show that this phase mixing introduces increasingly fine structure in the L-shell profile of $f(M, J, L, \phi, t)$ with time.

[21] In order to reveal the net effect of radial transport on the phase space density, an average over the drift phase was taken: $\langle f(M, J, L, t)\rangle = 1/2\pi \int f(M, J, L, \phi, t)d\phi$, and is shown as a function of time and L-shell in Figure 3b. This figure demonstrates the formation and growth of a localized peak (at $L \approx 6$, between 5 and 10 ULF periods after the source commencement) which cannot be explained by diffusion across L-shell. The final L-shell profile of $\langle f\rangle$, taken 40 wave periods after the source commencement, is shown in Figure 4. This figure also shows the average phase space density for a selection of different magnetic moments (from independent model executions using identical ULF wave and initial PSD parameters), all of which have drift-resonance locations on different L-shells. In each case a peak and corresponding trough in $\langle f\rangle$ is formed by coherent radial transport, centered at the location of the drift resonance, with an amplitude and width determined by the initial PSD variation with L-shell and the local wave amplitude.

[22] The formation of a radial peak in PSD by the mechanism described above depends on the duration of the ULF wave compared with the timescale for electrons to execute trapped orbits in the wave frame (i.e., the trapping period τ_{tr}). As mentioned earlier, the trapping period is not constant for all trapped electrons. In complete analogy with the nonlinear pendulum, it depends on the amplitude of the excursion from equilibrium of the trapped orbits, and asymptotically approaches a constant value for small amplitudes, in which case the electrons execute simple harmonic motion. Following a similar approach to that taken in the appendix of *Degeling et al.* [2006], and making the small angle approximation for the phase of an electron in the wave frame ($\psi = m\phi - \omega t$), the trapping frequency $\omega_{tr} = 2\pi/\tau_{tr}$ for these strongly trapped electrons can be approximated by,

$$\omega_{tr} \approx \left(\frac{\omega E_o}{2L_o R_E B}\left(1 + \frac{3}{\gamma^2}\right)\right)^{1/2} \tag{7}$$

where E_o, B, and γ are respectively the azimuthal electric field, magnetic field, and relativistic correction factor of electrons at the drift resonance location L_o.

[23] In order to characterize the peak formation in the L-shell profile of $\langle f\rangle$, a number of cases were run in which the peak ULF wave amplitude was scanned, and the duration of the wave was varied. The ULF wave amplitude was parameterized by the peak value of E_r occurring at the field line resonance, which was varied between 0 and 5 mV/m in 0.5 mV/m increments. The ULF wave duration was parameterized by the source decay constant τ_2, which was varied between 3 and 9 wave periods in 3 period increments. The magnetic moment of the electrons, the wave frequency, and all other parameters were left unchanged from the values used to produce Figure 2, such that the drift-resonance location remained at $L_o = 6.6$ in all cases. The results from these scans are summarized by the three contour plots shown in Figure 5, which correspond to the three values of τ_2 used. In each plot, the y-axis corresponds to the ULF wave amplitude, and the colors correspond to the final $\langle f\rangle$, taken 40 wave periods after the source commencement in each case.

[24] Scanning the ULF wave amplitude has the effect of increasing both the trapping width ΔL_{tr} and the trapping frequency ω_{tr}. The former effect gives rise to the roughly parabolic shape centered at $L = L_o$, marked out by the contour where $\langle f\rangle$ equals the unperturbed value of $\langle f\rangle$ at $L = L_o$ in Figures 5a, 5b, and 5c. Given that the ULF wave packet has a limited duration in time (approximated by τ_2), it could be expected that the effect of the changing trapping frequency with E_r in this figure would be to modulate the amplitude of the peak (and corresponding trough) in $\langle f\rangle$ as E_r is increased, such that the amplitude would attain a maximum value when $\omega_{tr}\tau_2 \approx 2\pi(N + 1/2)$ (where $N = 0$,

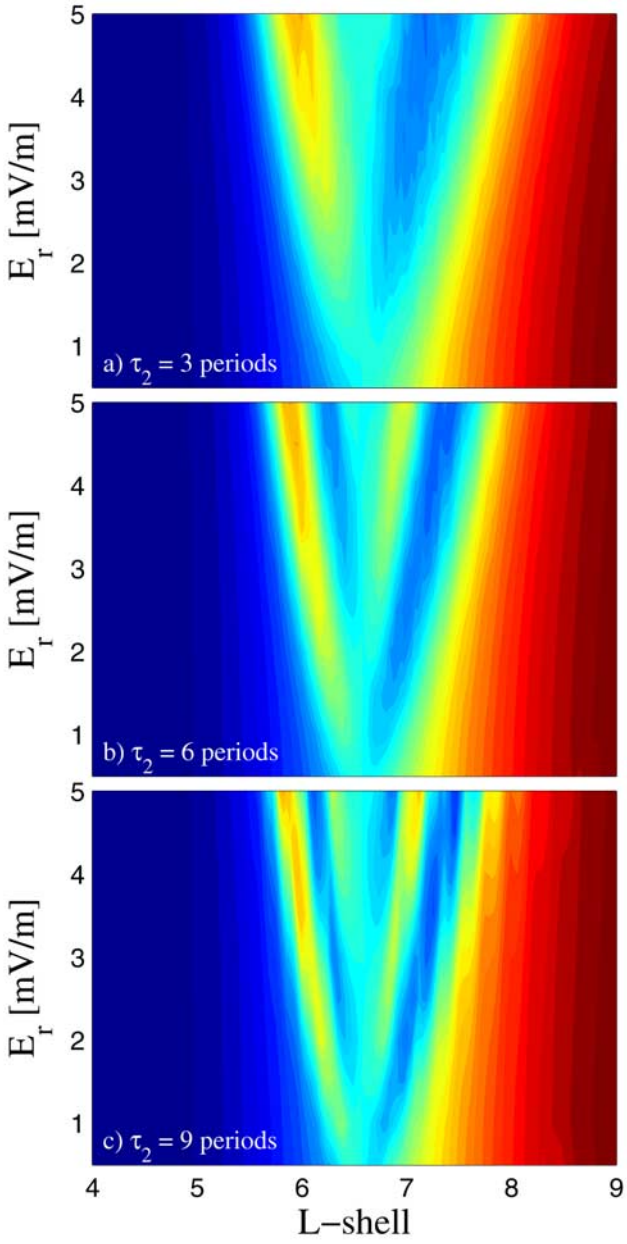

Figure 5. (a–c) Contour plots showing the final $\langle f \rangle$ profile after 40 wave periods, as the ULF wave amplitude is increased. The y-axis scale corresponds to the peak radial electric field at the FLR location. The duration of the ULF wave is scanned from Figure 5a to 5c by increasing the decay timescale of the source from 3 to 9 wave periods.

1, 2, . . .), and a minimum value when $\omega_{tr}\tau_2 \approx 2\pi N$. Figure 5 qualitatively shows this expected behavior. For example (concentrating on L-shells below L_o in the following), the peak in $\langle f \rangle$ occurring at the lowest L-shell corresponds to $\omega_{tr}\tau_2 \approx \pi$ in Figures 5a, 5b, and 5c, the adjacent trough at higher L-shell visible in Figures 5b and 5c corresponds to $\omega_{tr}\tau_2 \approx 2\pi$, and the next adjacent peak visible only in Figure 5c corresponds to $\omega_{tr}\tau_2 \approx 3\pi/2$. This figure illustrates that the trapping frequency is only approximated by equation (7) close to the resonance, and decreases continuously as $|L - L_o|$ increases, reaching zero when $|L - L_o| = \Delta L_{tr}$. For this reason, the peak (and associated trough) in $\langle f \rangle$ corresponding to a given N occurs at a greater $|L - L_o|$, and asymptotically approaches ΔL_{tr} as E_r is increased.

[25] These figures show that multiple peaks in $\langle f \rangle$ with L-shell may be produced by coherent radial transport due to the drift resonance mechanism, depending on the duration and amplitude of the ULF wave.

5. Discussion: Implications for the Interpretation of in Situ Observations

[26] It is important to emphasize that the results of the previous section, showing the formation of one or more localized peaks in $\langle f \rangle$ with L-shell, are qualitatively different from scenarios involving radial diffusion with a time dependent external source of electrons. For example, *Selesnick and Blake* [2000] demonstrate that a peak in $f(M, J, L, t)$ develops at lower L-shell with time using a simple radial diffusion model if the high L-shell boundary condition for f provides a transient pulse of electrons. As shown by *Selesnick and Blake* [2000, Plate 7, bottom] (a color-coded plot of f versus L-shell and time), a monotonic distribution with L-shell develops initially while the source at the outer boundary exists, and a local peak at lower L-shell develops only after the high L-shell source is extinguished. This local peak strictly decays in amplitude with time, as indicated in the figure by the contours of constant f (represented by colors in the figure), which are all open to the high L-shell upper boundary. Similar results would also be obtained if L-dependent losses that increase with L-shell are used. This contrasts with contours of constant $\langle f \rangle$ in Figure 3b, which are closed in the vicinity of the peak developing close to $L = 6$, indicating local growth of the peak with time.

[27] It is usually assumed that an internal source of phase space density at constant invariants, such as arising from a VLF wave acceleration process which violates the first invariant, is responsible for growing peaks in PSD (for example, a model similar to that shown by *Selesnick and Blake* [2000, Plate 7, top]). As shown in our Figure 3b, a peaked $\langle f \rangle$ distribution as a function of L can be generated through radial transport generated by the interaction with coherent ULF waves. This leads to the conclusion that contrary to the standard interpretation, in situ measurements by satellites of the gradient of $f(M, J, L, t)$ with L, and even the time evolution of this profile, may be insufficient to distinguish between internal and external electron acceleration mechanisms, unless information on the (ULF or VLF) waves presumably causing the acceleration is also obtained.

[28] It is important to consider in some detail what the electron flux time series measured by a satellite would look like, if this nondiffusive transport mechanism were in fact taking place. For example, if we were to plot the evolution of the measured phase space density profile with time, would we see an image more closely resembling Figure 3a or 3b? According to *Schulz and Lanzerotti* [1974], the coarse resolution provided by the finite width of energy bins and acceptance angles of satellite particle detectors places a short lifetime on gyrophase, bounce phase, and drift phase information obtainable from electron flux time series, due to phase-mixing. This means that variations in observed electron flux that occur on a timescale much longer than the phase

mixing timescale may be interpreted as variations in the average phase space density $\langle f(M, J, L, t)\rangle$. This is the interpretation taken by *Green and Kivelson* [2004] and *Selesnick and Blake* [2000] when obtaining $f(M, J, L, t)$ from Polar satellite observations. However, such an interpretation may not always be applicable in the presence of narrow band ULF waves, where perturbations to electron PSD over a range in M, J, and L can remain coherent while the ULF wave amplitude is significant. In this case the electrons in drift-resonance with the wave, especially the strongly trapped electrons undergoing simple harmonic motion, remain phase-correlated, such that ULF modulations in electron flux may be visible. Such an event would be distinguished from a drift echo by the observation of an approximately constant modulation frequency over a range of energy bins (corresponding to the drift-resonance trapping width), and phase correlation with an independently observed ULF wave. Examples of such signatures in LANL electron flux and GOES magnetometer data have been reported for ULF oscillations below 1 mHz [*Lessard et al.*, 2003]. Of course, on timescales longer than the ULF wavetrain the loss of phase information in f will develop over the phase mixing timescale and the interpretation of *Schulz and Lanzerotti* [1974] becomes applicable.

[29] Last, the impact of some of the assumptions made in the electron dynamics and ULF wave model should be discussed, in particular the effect of neglecting the convection electric field and assuming a dipole magnetic field. The relaxation of these assumptions would break the azimuthal symmetry in the zeroth-order drift paths of the electrons and lead to the introduction of additional drift resonances, as found by *Elkington et al.* [1999]. If the asymmetry is sufficiently large then overlap between these resonances may lead to globally stochastic dynamics; however, it is not at all clear whether this would lead to diffusive behavior, and preclude the formation and growth of localized phase space density peaks. As discussed by *Degeling et al.* [2006], this requires that the timescale for phase decorrelation is significantly shorter than the ULF wave duration. A further effect of azimuthal asymmetry in the geomagnetic field is the alteration to the shear wave eigenfunctions with MLT, as discussed by *Kabin et al.* [2007], which may strongly affect electron dynamics close to a field line resonance. Another particularly interesting question is how the introduction of fluctuations in the ULF amplitude, and a broadband noise floor affect the electron dynamics. As discussed in the introduction, according to *Sagdeev and Galeev* [1969] the dynamics should remain nondiffusive as long as the spread in drift resonance locations associated with the fourier components of the ULF fluctuations is less than the combined trapping width. These questions will be addressed in future work.

6. Conclusion

[30] The drift-resonance interaction between relativistic, equatorially mirroring electrons and a ULF wave packet in the Pc-5 frequency range is investigated. Using a dipole wave model with a time-dependent wave amplitude, it is demonstrated that bursts of narrow-band ULF waves can produce one or more localized peaks in electron phase space density f by coherent radial transport via the drift resonance mechanism. During the early time evolution, where the wave amplitude is large, these peaks have azimuthal structure (with a periodicity given by the azimuthal mode number of the ULF wave) in addition to the L-shell structure. Averaging over the azimuthal drift phase reveals that the effect of the drift resonance on the average phase space density $\langle f\rangle$ expressed as a function of the invariants M, J, L, and time is to give rise to a growing peak in L, which is qualitatively similar to that expected from an internal source acceleration mechanism breaking the first invariant. During the interval of ULF wave activity, the electrons comprising the peaks in f remain phase-correlated with the wave and will give rise to measurable temporal modulations in electron flux similar to drift echoes. Following the decay of the wave fields, these modulations will be attenuated due to the phase mixing effect inherent in particle detectors with finite energy resolution, such that f inferred from the measured electron flux evolves towards the average phase space density $\langle f\rangle$. We therefore conclude that in situ measurements of average phase space density gradients by satellite are insufficient by themselves to determine the electron acceleration mechanism. However, additional information from corroborating wave field measurements may be able to remove this ambiguity.

Appendix A: Details of the ULF Wave Model

[31] From equation (3) the α and β components of the wave displacement are governed by

$$\frac{h_\beta^2}{v_A^2}\frac{\partial^2}{\partial t^2}\left(\frac{\xi_\beta}{h_\beta}\right) - \frac{\partial}{\partial\mu}\left(\frac{1}{h_\alpha^2}\frac{\partial}{\partial\mu}\left(\frac{\xi_\beta}{h_\beta}\right)\right) = \frac{\partial}{\partial\beta}\left(\frac{\partial}{\partial\alpha}\left(\frac{\xi_\alpha}{h_\alpha}\right) + \frac{\partial}{\partial\beta}\left(\frac{\xi_\beta}{h_\beta}\right)\right) \tag{A1}$$

$$\frac{h_\alpha^2}{v_A^2}\frac{\partial^2}{\partial t^2}\left(\frac{\xi_\alpha}{h_\alpha}\right) - \frac{\partial}{\partial\mu}\left(\frac{1}{h_\beta^2}\frac{\partial}{\partial\mu}\left(\frac{\xi_\alpha}{h_\alpha}\right)\right) = \frac{\partial}{\partial\alpha}\left(\frac{\partial}{\partial\alpha}\left(\frac{\xi_\alpha}{h_\alpha}\right) + \frac{\partial}{\partial\beta}\left(\frac{\xi_\beta}{h_\beta}\right)\right) \tag{A2}$$

and are equivalent to the wave equations of *Radoski* [1967].

[32] Taking a spectral approach, the general solutions to the above equations can be written in the form of a sum over locally evaluated poloidal and toroidal eigenfunctions $f_{\alpha n}$ and $f_{\beta n}$ multiplied by time-dependent and α-dependent amplitudes $A_{\alpha n}$ and $A_{\beta n}$.

$$\frac{\xi_\alpha}{h_\alpha} = \sum_{n=1}^{\infty} A_{\alpha n}(\alpha, t) f_{\alpha n}(\alpha, \mu) e^{i(m\beta-\omega t)}. \tag{A3}$$

$$\frac{\xi_\beta}{h_\beta} = \sum_{n=1}^{\infty} A_{\beta n}(\alpha, t) f_{\beta n}(\alpha, \mu) e^{i(m\beta-\omega t)} \tag{A4}$$

[33] The eigenfunctions and their corresponding eigenfrequencies $\omega_{\alpha n}(\alpha)$ and $\omega_{\beta n}(\alpha)$ are given by

$$\left(\frac{\omega_{\alpha n}^2 h_\alpha^2}{v_A^2} + \frac{\partial}{\partial\mu}\left(\frac{1}{h_\beta^2}\frac{\partial}{\partial\mu}\right)\right) f_{\alpha n} = 0 \tag{A5}$$

$$\left(\frac{\omega_{\beta n}^2 h_\beta^2}{v_A^2} + \frac{\partial}{\partial\mu}\left(\frac{1}{h_\alpha^2}\frac{\partial}{\partial\mu}\right)\right) f_{\beta n} = 0 \tag{A6}$$

[34] These are the poloidal and toroidal eigenmode equations treated analytically for certain v_A profiles by *Allan and Knox* [1979] and *Ozeke and Mann* [2004] (see also *Radoski* [1967]). Ionospheric boundary conditions with finite height-integrated Pedersen conductivity Σ_p are assumed, such that $-i\omega\ \mu_o\ \Sigma_p\ h_\mu f_{\alpha,\beta} = \partial/\partial\mu(f_{\alpha,\beta})$ at the boundaries. These eigenfunctions are normalized according to the following conditions:

$$\alpha^2 \int_{-\mu_m}^{\mu_m} \frac{h_\alpha^2}{u_A^2} f_{\alpha k} f_{\alpha n} d\mu = \delta_{kn} \tag{A7}$$

$$\int_{-\mu_m}^{\mu_m} \frac{h_\beta^2}{u_A^2} f_{\beta k} f_{\beta n} d\mu = \delta_{kn} \tag{A8}$$

[35] We assume the local eigenfunctions only weakly depend on α. This is true as long as the ionosphere is highly conductive, such that $\Sigma_p \gg \Sigma_p^{crit}$, where $\Sigma_p^{crit} = 1/\mu_o v_{AI}$ (where v_{AI} is the Alfvén speed evaluated at the ionosphere [*Ozeke and Mann*, 2004]). Therefore for the purposes of this article we use $\Sigma_p = 10\Sigma_p^{crit}$ in all cases.

[36] Following the methods of *Rankin and Tikhonchuk* [2001] and *Walker* [1980], we make the expedient assumption that the solutions are dominated by the local fundamental eigenfunctions, and hence the index n takes the value of one in the following and will be dropped for brevity. The limitations of this assumption will be discussed at the end of this section. The fundamental eigenfunctions $f_{\alpha,\beta}$ are numerically computed for various α, making the approximation that $v_A(\alpha, \mu) = u_A(\mu)\, w_A(\alpha)$, where u_A and w_A are specified, based on the dipole magnetic field and an assumed plasma mass density profile. The remaining task is to solve for the amplitudes A_α and A_β in response to a time-dependent driver at the outer L-shell boundary (representing the magnetopause).

[37] We take the slowly varying envelope approximation for the time-dependence [*Rankin and Tikhonchuk*, 2001] and assume that A_α and A_β vary much more rapidly with α than f_α and f_β [*Walker*, 1980]. Multiplying the resulting wave equations by f_α and f_β, respectively, and integrating along field lines gives

$$2i\omega\dot{A}_\alpha + \left(\omega^2 - \omega_\alpha^2\right)A_\alpha = -w_A^2\alpha^4\left(\Omega_{\alpha\alpha}A_\alpha'' + im\Omega_{\alpha\beta}A_\beta'\right) \tag{A9}$$

$$2i\omega\dot{A}_\beta + \left(\omega^2 - \omega_\beta^2\right)A_\beta = w_A^2\alpha^2\left(-im\Omega_{\beta\alpha}A_\alpha' + m^2\Omega_{\beta\beta}A_\beta\right) \tag{A10}$$

where the dots and dashes represent time and α-derivatives, respectively, and

$$\Omega_{j,k} = \int_{-z_m}^{z_m}\left(\frac{1+3z^2}{(1-z^2)^3}\right) f_j f_k dz \tag{A11}$$

(where the subscript labels j and k are either α or β). Here, integrals along field lines are written in terms of $z = \cos(\theta)$, such that $\mu = \alpha^2 z/(1-z^2)^2$, and the ionospheric boundary is assumed to be at $r = 1R_E$, such that $z_m = (1 - \alpha R_E)^{1/2}$. For the purposes of this model, the plasma mass density profile along field lines is assumed to vary as r^{-6}, in which case, $u_A = 1 + 3z^2$ and the toroidal mode eigenfunction f_β becomes analytic [*Allan and Knox*, 1979]. The equatorial Alfvén speed variation across L-shell is assumed to have the form $w_A = w_{Ao}\alpha^P$, where $P = 1$ represents a typical mass density variation with L-shell outside the plasmapause of α^4, and w_{Ao} is a constant.

[38] Equations (A9) and (A10) subject to appropriate boundary conditions are solved using a fully implicit finite differencing scheme, which involves the inversion of a pentadiagonal matrix equation at each time step using a generalization of the Thomas algorithm, given by *Engeln-Muellges and Uhlig* [1996]. The inner and outer α boundary conditions are as follows: Evanescent solutions are expected at the boundary close to the Earth (maximum α, placed earthward of the compressional wave turning point), hence the condition $A'_\alpha + \nu A_\alpha = 0$ is used (and similarly for A_β). An incident plane wave source is included at the outer L-shell boundary (minimum α) by expressing A_α and A_β as the superposition of incident and reflected waves, such that $A'_\alpha + ikA_\alpha = 2ikA_{\alpha s}$ (and similarly for A_β), where $A_{\alpha s}(t)$ (and $A_{\beta s}(t)$) represent the time-dependent source amplitude. The constants k and ν are obtained by applying the WKB approximation at boundary locations. Both $A_{\alpha s}(t)$ and $A_{\beta s}(t)$ are specified to have the form $e^{-t/\tau 2}(1 - e^{-t/\tau 1})$, where τ_1 and τ_2 are the source rise and decay times, respectively.

[39] The limitations of the assumption that the fundamental eigenfunctions f_α and f_β are not coupled to higher harmonics is apparent from the plot of $b_\parallel$ shown in Figure 1c, which shows a significant peak at the location of the FLR. The solution should be Alfvénic at the FLR, such that the right-hand side of equation (A2) (which amounts to the α-derivative of $b_\parallel$) should be very close to zero at this location [*Walker*, 1980]. The differences in f_α and f_β along the magnetic field prevent the required cancellation of terms in this model.

[40] **Acknowledgments.** The authors would like to acknowledge many useful discussions with Jonathan Rae, Clare Watt, and Paul Loto'aniu during the preparation of this manuscript. This work is supported by the Canadian Space Agency and by the National Scientific and Engineering Research Council.

[41] Zuyin Pu thanks the reviewers for their assistance in evaluating this paper.

References

Allan, W., and F. B. Knox (1979), A dipole model for axisymmetric Alfvén waves with finite ionospheric conductivities, *Planet. Space Sci.*, *31*, 323.

Allan, W., and E. M. Poulter (1992), ULF waves-their relationship to the structure of the Earth's magnetosphere, *Rep. Prog. Phys.*, *55*, 533.

Brizard, A. J., and A. A. Chan (2001), Relativistic bounce averaged quasi-linear diffusion equation for low frequency electromagnetic fluctuations, *Phys. Plasmas*, *8*, 4762.

Degeling, A. W., R. Rankin, K. Kabin, R. Marchand, and I. R. Mann (2006), The effect of ULF compressional modes and field line resonances on relativistic electron dynamics, *Planet. Space Sci.*, *55*, 731, doi:10.1016/j.pss.2006.04.039.

Elkington, S. R., M. K. Hudson, and A. A. Chan (1999), Acceleration of relativistic electrons via drift-resonant interaction with toroidal-mode Pc-5 ULF oscillations, *Geophys. Res. Lett.*, *26*, 3273.

Elkington, S. R., M. K. Hudson, and A. A. Chan (2003), Resonant acceleration and diffusion of outer zone electrons in an asymmetric geomagnetic field, *J. Geophys. Res.*, *108*(A3), 1116, doi:10.1029/2001JA009202.

Engeln-Muellges, G., and F. Uhlig (1996), *Numerical Algorithms With C*, chap. 4, Springer, Berlin.

Falthammer, C. G. (1965), Effects of time dependent electric fields on geomagnetically trapped radiation, *J. Geophys. Res.*, *70*, 2503.

Fenrich, F. R., J. C. Samson, G. Sofko, and R. A. Greenwald (1995), ULF high- and low- m field line resonances observed with the Super Dual Auroral Radar Network, *J. Geophys. Res.*, *100*, 21,535.

Friedel, R. H. W., G. D. Reeves, and T. Obara (2002), Relativistic electron dynamics in the inner magnetosphere-A review, *J. Atmos. Sol. Terr. Phys.*, *64*, 265.

Green, J. C., and M. G. Kivelson (2004), Relativistic electrons in the outer radiation belt: Differentiating between acceleration mechanisms, *J. Geophys. Res.*, *109*, A03213, doi:10.1029/2003JA010153.

Horne, R. B., et al. (2005), Wave acceleration of electrons in the Van Allen radiation belts, *Nature*, *437*, 227, doi:10.1038/nature03939.

Kabin, K., R. Rankin, I. R. Mann, A. W. Degeling, and R. Marchand (2007), Polarization properties of standing shear Alfvn waves in non-axisymmetric background magnetic fields, *Ann. Geophys.*, *25*, 815.

Lessard, M. R., J. Hanna, E. F. Donovan, and G. D. Reeves (2003), Evidence for a discrete spectrum of persistent magnetospheric fluctuations below 1 mHz, *J. Geophys. Res.*, *108*(A3), 1125, doi:10.1029/2002JA009311.

Loto'aniu, T. M., I. R. Mann, L. G. Ozeke, A. A. Chan, Z. C. Dent, and D. K. Milling (2006), Radial diffusion of relativistic electrons into the radiation belt slot region during the 2003 Halloween geomagnetic storms, *J. Geophys. Res.*, *111*, A04218, doi:10.1029/2005JA011355.

Mathie, R. A., and I. R. Mann (2000), A correlation between extended intervals of ULF wave power and storm-time geosynchronous relativistic flux enhancements, *Geophys. Res. Lett.*, *27*, 3261.

Northrop, T. G. (1963), *The Adiabatic Motion of Charged Particles*, John Wiley, New York.

Nunn, D. (1993), A novel technique for the numerical simulation of hot collision-free plasma: Vlasov Hybrid Simulation, *J. Comput. Phys.*, *108*, 180.

O'Brien, T. P., K. R. Lorentzen, I. R. Mann, N. P. Meredith, J. B. Blake, J. F. Fennell, M. D. Looper, D. K. Milling, and R. R. Anderson (2003), Energization of relativistic electrons in the presence of ULF power and MeV microbursts: Evidence of dual ULF and VLF acceleration, *J. Geophys. Res.*, *108*(A8), 1329, doi:10.1029/2002JA009784.

Ozeke, L. G., and I. R. Mann (2004), Modeling the properties of guided poloidal Alfvén waves with finite asymmetric ionospheric conductivities in a dipole field, *J. Geophys. Res.*, *109*, A05205, doi:10.1029/2003JA010151.

Radoski, H. R. (1967), A note on oscillating field lines, *J. Geophys. Res.*, *87*, 1703.

Rae, I. J., et al. (2005), Evolution and characteristics of global Pc-5 ULF waves during a high solar wind speed interval, *J. Geophys. Res.*, *110*, A12211, doi:10.1029/2005JA011007.

Rankin, R., and V. T. Tikhonchuk (2001), Linear and nonlinear dispersive effects on magnetospheric field line resonances, *Phys. Chem. Earth C*, *26*, 121.

Riley, P., and R. A. Wolf (1992), Comparison of diffusion and particle drift descriptions of radial transport in the Earth's inner magnetosphere, *J. Geophys. Res.*, *97*, 16,865.

Roederer, J. G. (1970), *Dynamics of Geomagnetically Trapped Radiation*, Springer, New York.

Rostoker, G., S. Skone, and D. N. Baker (1998), On the origin of relativistic electrons in the magnetosphere associated with some goemagnetic storms, *Geophys. Res. Lett.*, *25*, 3701.

Sagdeev, R. Z., and A. A. Galeev (1969), *Nonlinear Plasma Theory*, Benjamin, New York.

Schulz, M., and L. J. Lanzerotti (1974), *Particle Diffusion in the Radiation Belts*, Springer, New York.

Selesnick, R. S., and J. B. Blake (2000), On the source location of radiation belt relativistic electrons, *J. Geophys. Res.*, *105*, 2607.

Ukhorskiy, A. Y., K. Takahashi, B. J. Anderson, and H. Korth (2005), Impact of toroidal ULF waves on the outer radiation belt electrons, *J. Geophys. Res.*, *110*, A10202, doi:10.1029/2005JA011017.

Ukhorskiy, A. Y., B. J. Anderson, K. Takahashi, and N. A. Tsyganenko (2006a), Impact of ULF oscillations in solar wind dynamic pressure on the outer radiation belt electrons, *Geophys. Res. Lett.*, *33*, L06111, doi:10.1029/2005GL024380.

Ukhorskiy, A. Y., B. J. Anderson, P. C. Brandt, and N. A. Tsyganenko (2006b), Storm time evolution of the outer radiation belt: Transport and losses, *J. Geophys. Res.*, *111*, A11S03, doi:10.1029/2006JA011690.

Walker, A. D. M. (1980), Modelling of Pc5 pulsation structure in the magnetosphere, *Planet. Space Sci.*, *28*, 213.

A. W. Degeling, K. Kabin, I. R. Mann, L. G. Ozeke, and R. Rankin, Department of Physics, University of Alberta, Edmonton, AB, Canada T6G 2G7. (degeling@phys.ualberta.ca)